Icarus **154**, 432–448 (2001)
doi:10.1006/icar.2001.6683, available online at http://www.idealibrary.com on IDEAL®

Equilibrium Configurations of Solid Cohesionless Bodies

K. A. Holsapple

Department of Aeronautics and Astronautics, University of Washington, 352400, Seattle, Washington 98195
E-mail: holsapple@aa.washington.edu

Received January 12, 2001; revised June 6, 2001

The bodies of the Solar System exist in a variety of irregular shapes. Studies of those shapes are conducted to infer information about the internal composition, structure, and history of those bodies. However, such inferences require knowing how the composition and structure or history relates to the shape and internal forces. That connection is known only for fluid bodies, where the permissible equilibrium states were discovered centuries ago by Newton, Maclaurin, Jacobi, Poincaré, and Roche. While others have given results for linear elastic solid bodies, the elastic problem is not uniquely posed, since elastic solutions depend on an implicit assumption about the existence and shape of an initial stress-free state. The present states of Solar System bodies are a culmination of complicated past histories, possibly involving collisions, disruption, melting, accumulation, and large-scale yielding and reshaping. Such processes create underlying residual stress fields that cannot be known.

Here I present an approach in the same spirit as for the fluid bodies: limits on equilibrium shapes are determined. Results are obtained for a cohesionless elastic–plastic solid with a Mohr–Coloumb yield criteria. That model is commonly used in soil mechanics and is appropriate for "rubble pile" reaccumulated asteroids that have negligible cohesive forces. It is possible to determine *limit* equilibrium stress fields and shapes that are independent of past histories, using the approaches of limit analyses of elastic–plastic theories. The results show that for these bodies there exists a *region* of permissible combinations of shape and spin rates, centered about the unique equilibrium fluid states of Maclaurin and Jacobi.

The database on asteroids is compared to those equilibrium states. Few asteroids are outside the limit shape envelopes according to this theory.

The application of the analysis to Phobos is also presented, assuming that the rubble-pile model is appropriate. The deformation that would occur as it moves closer to Mars is determined; it is shown to be unstable and globally catastrophic at about 2.1 Mars radii.

Key Words: **asteroids; celestial mechanics; solid bodies; tides; satellites of Mars.**

1. INTRODUCTION

The determination of equilibrium shapes of fluid bodies with gravitational, centrifugal and/or tidal forces is a classical problem that has spanned over three centuries. Newton (1687) determined that the shape of an almost spherical fluid Earth with gravitational and rotational forces is a slightly oblate spheroid. Maclaurin (1742) extended the work to discover the existence of equilibrium oblate spheroidal shapes with large ellipticity for rotating bodies with self-gravity, now called the "Maclaurin spheroids." Jacobi (1834) discovered the "Jacobi ellipsoids": equilibrium ellipsoidal shapes with three unequal axes. Others extended the work to allow for internal rotational motions of a fluid body. Roche (1850) considered the tidal forces during an orbit around a parent body and determined that there is a limit to the orbit radius, the famous "Roche limit," inside of which there are no equilibrium solutions. Poincaré (1885) discovered other pear-shaped, nonellipsoidal possibilities for equilibrium. Chandrasekhar (1969) gives a complete exposition of these classical works.

The assumption of fluid behavior may be warranted for gaseous bodies; but for Solar System bodies the assumption of fluid behavior is generally unwarranted, and these results are interesting only as limit cases. To study the breakup of solid bodies by tidal forces, Jeffreys (1947) and Õpik (1950), neglecting self-gravitation and spin forces, and looking only at the force across an entire cross section for rigid spherical bodies, determined Roche limits for solids, using either a maximum tensile or maximum shear force criteria for failure. A recent paper by Davidsson (1999) included all of gravitational, spin, and tidal forces but still assumed a rigid spherical body and still used only averaged total forces across certain cross sections. Davidsson compared those forces to either tensile or shear force criteria to determine tidal limits and spin limits. The consideration of force averages across cross-sectional planes has a great advantage in that the force solution is statically determined, but the approach suffers from the lack of knowledge of actual stress variations across that cross section and, as a consequence, imprecise knowledge of reasonable stress failure criteria.

Sekiguchi (1970) and Aggarwal and Oberbeck (1974) revisited the Jeffreys and Õpik theories. Aggarwal and Oberbeck assumed an incompressible but otherwise elastic material and retained the spherical assumption. Following Love (1944), they assumed an initial state of hydrostatic pressure. They considered both an impacting body (no spin) and an orbiting, spin-locked body. They compare their results to those of Roche and claim that the significant differences are due to nonlinearities in fluid

0019-1035/01 $35.00

behavior, although nowhere in Roche's approach is there any use of constitutive equations. The difference should instead be attributed to their assumption of a spherical body, while the fluid solutions exist only for certain significantly nonspherical ellipsoidal bodies.

Dobrovolskis (1982) considered the equilibrium of elastic triaxial ellipsoids with gravitational, spin, and tidal forces; Slyuta and Voropaev (1997) considered only prolate spheroids with self-gravitation. Both papers presented complete elastic stress, strain, and displacement fields. Since they lead to elastic solutions, both of these approaches implicitly assume deformation from an initial globally stress-free state.

For all of these solutions, there are equilibrium solutions for arbitrary shape and spin rate. The elastic solutions are unique only from a given initial configuration. Thus the search shifts from looking for shapes that are possible to assuming a shape and initial state and deriving the stress, strain, and displacement field imposed by the gravitational, rotational, or tidal forces. Then failure is an additional consideration, based upon a comparison of the elastic stress state to some stress failure or flow criteria for the onset of plastic failure or flow. The consequences of that "failure" are not easily determined, and disagreements have arisen over that point.

For a general solid body, there is generally a multitude of equilibrium stress solutions, and the one that also satisfies the equations of strain compatibility (or is derived from smooth displacement fields) is the unique *elastic* solution to the problem, assuming an initial stress-free state. That is, the stress field is statically indeterminate, and considerations of displacements from some initial state are necessary to make the solution unique. In elasticity those deformation considerations are imposed by the assumption of a smooth deformation from an initial stress-free state, or, equivalently, by the equations of strain compatibility on the strains calculated from the stresses using Hooke's law.

In this author's view, both the force approaches and the elastic approaches have serious deficiencies. In the former, it is the lack of detail about actual stress distributions and the uncertainty over failure criteria for averaged forces. In the latter elastic methods, there are two deficiencies. The first is the implicit need to choose the initial state; the second is the inability to consider subsequent deformation when the first yield is reached. The stress-free initial state assumption gives solutions for a body that was assembled with no stresses whatsoever, followed by the application of the gravitational, rotational, and tidal forces, to give displacement and stress fields from the initial stress-free reference state. Love (1944) comments on that problem. In his discussion of the deformation of the Earth under spin, he states: "All such applications are beset by the difficulty which has been noted in Article 75, viz.: that even when the effects of rotation and disturbing forces are left out of account, the Earth is in a condition of stress, and the internal stress is much too great to permit of the direct application of the mathematical theory of superposable small strains." He gives a reference to Chree (1891) for that observation. However, he then sidesteps the problem by assuming that the initial stress is only a hydrostatic pressure, in equilibrium with the gravitational forces. Dobrovolskis (1982) does not consider any initial state but also correctly notes that same problem, when interpreting aspects of his elastic solution. He states: "Obviously, it is unrealistic to imagine a planet or satellite fully assembled when self-gravitation is abruptly turned on, leading to a sudden collapse of its surface. This difficulty can be mitigated in the case of an incompressible solid, but such an idealization (besides failing to simplify the stress calculations) is somewhat unrealistic even for chondritic material."

While assuming a stress-free initial state is appropriate for man-made structures such as airplanes or bridges, which are built and then loaded, it does not seem suitable for Solar System bodies that form and are modified while the loads are always present. If the body has undergone any readjustments, reshaping, or disruption during its history, there will generally not be a global stress-free reference state. Instead there will exist inelastic strains, and any global state with no forces would have significant internal residual stresses. A determination of stress fields in an elastic body of a given shape, subsequently compared to some elastic limit, does not give a limit configuration; it simply gives the state requiring inelastic flow and a change of internal stresses. Then later deformations will not be from a global stress-free state.

The more general inelastic problem must be analyzed using a complete inelastic theory; and, since the deformations of interest would be expected to significantly change the body's shape, the analysis would require a finite deformation theory. However, there are powerful approaches used in plasticity theories that circumvent the need to know the past history: the so-called limit analyses. In these approaches one seeks the *maximum* load which, for a given shape, can be withstood without unconstrained plastic flow. That approach is used here. The interest is then to determine meaningful equilibrium *limit* solutions for solid bodies, and in particular for bodies consisting of materials such as soils, rocks, ices, or metals, whether coherent or loosely bound assemblages of small pieces ("rubble piles").

In Earth-bound studies of geological materials, in the fields of soil and rock mechanics, it is universally accepted that appropriate material behavior descriptions require elastic–plastic theories. A further basic tenet for many particulate (soil or gravel) or solid (rock) geological materials is that the shear yield stress on any plane increases with the normal pressure on that plane. The simplest criterion of that type is the well-known Mohr–Coloumb (MC) yield criterion, determined solely by a cohesion Y and an angle of friction ϕ. Also required is some "flow rule" to determine the flow: some prescription of the plastic deformations that occur when the stresses meet or exceed the yield criteria. These flow rules are commonly given in a rate or incremental form. Then, in principle, one can trace a particular loading (or formation) history and incrementally determine the resulting stress and strain fields.

Such an analysis is clearly complex, and the outcome will depend on many of the details of the history, which cannot be

known for a given body. There are an infinity of equilibrium solutions, corresponding to the infinity of possible histories. Thus, such an analysis is also of limited usefulness. However, as stated above, one can in many cases in elastic–plastic theories determine unique limit loads without considerations of or knowledge of past body history, using the limit load theorems for the theory.

Here, that limit problem is partly solved. For a Mohr–Coloumb material with zero cohesion, such limit solutions are found for arbitrary ellipsoidal bodies with self-gravitational and/or tidal and rotational forces. The solutions provide the limit loads for a given configuration and also the limit configurations for which the body can exist in equilibrium without yield. In addition, at those limits the flow rules can be used to determine whether the deformation patterns would tend to lead to catastrophic disruption or to evolution to a new equilibrium state.

This model is suitable for a body with a negligible-strength rubble-pile structure. It is commonly used for studies in soil mechanics for dry sand, gravel, and "dirt" of moderate porosity, specifically, for materials consisting of mineral grains with grain density on the order of 3 to 4 g/cm^3 having a bulk density of perhaps 1.5 to 2.5 g/cm^3. Consequently, the model can be said to be appropriate for "gravel balls" in space. It would not be appropriate for a very fragile porous structure held together by weak cohesive forces, such as may be the case for comets. It is also a continuum model and so would not be a good model for an assemblage of a small number of rocks, which may be more appropriately modeled using "n-body" approaches such as that by Richardson *et al*. (1998).

For such a cohesionless material, the yield criterion is characterized by a single material property, the angle of friction ϕ. In the limit case where that angle is zero, the description is that of a fluid, with equal pressure stresses required in all directions. Consequently, all of the special fluid cases of Maclaurin, Jacobi, and Roche, where only special equilibrium shapes are possible, are exactly included in the results. For nonzero friction angles, there are ranges of possible shapes, which are presented. The results are compared to the database of the shapes and spins of known asteroids. It is found that, with very few exceptions, all can exist in their present states as cohesionless rubble-pile materials with very modest values for the angle of friction.

The structure of this paper is as follows. Section 2 begins with a general polynomial solution for the stress components in terms of 15 constants. The equilibrium equations and the zero-stress boundary conditions are shown to determine 12 constants, no matter what constitutive equation is to be used. Then the final three can be found for an elastic result; or, in the approach here, the final three are determined by constraints of the Mohr–Coloumb yield condition. The final resulting form for the stresses is then determined for a general quadratic body force potential; those are given in Eq. (10).

Since this beginning polynomial form is only a particular solution, it must be proved to be unique. In Section 3 this question is posed and answered within the context of limit solutions of elastic–plastic theories. Readers unfamiliar with those theories may want to take those discussions for granted.

Section 4 then gives the primary results: plots of curves of permissible spin and shape combinations for various values of the friction angle of the yield criteria. The shapes and spins from the database of asteroids are compared to those limits in Section 5. Finally, the application of the analysis to Phobos is presented in Section 6.

2. EQUILIBRIUM STATES

The stresscs σ_{ij} in any body in equilibrium with body forces b_i must satisfy the three stress equilibrium equations. In an indicial summation notation using Cartesian coordinates x_i they are given as:

$$\frac{\partial}{\partial x_j}\sigma_{ij} = -\rho b_i \tag{1}$$

where ρ is the mass density, which is assumed to be constant.

The mutual gravitational forces, centrifugal forces, and tidal forces for the body are obtained from a potential function V as

$$b_i = -\frac{\partial V}{\partial x_i} \tag{2}$$

For ellipsoidal bodies, and, assuming a large distant source for the tidal forces (first order terms only), the potential is quadratic in the coordinates. Using now an x, y, z coordinate notation it has the form:

$$V = -V_0 + k_x x^2 + k_y y^2 + k_z z^2 \tag{3}$$

so that the body forces from Eq. (2) are linear in the three coordinates.

As a consequence of the symmetry about the three axes, a particular solution to the equilibrium equations can be obtained starting from quadratic forms given as

$$\begin{aligned}
\sigma_{\mathrm{x}} &= k_1 + k_2 x^2 + k_3 y^2 + k_4 z^2 \\
\sigma_{\mathrm{y}} &= k_5 + k_6 x^2 + k_7 y^2 + k_8 z^2 \\
\sigma_{\mathrm{z}} &= k_9 + k_{10} x^2 + k_{11} y^2 + k_{12} z^2 \\
\tau_{\mathrm{xy}} &= k_{13} xy \\
\tau_{\mathrm{xz}} &= k_{14} xz \\
\tau_{\mathrm{xz}} &= k_{15} yz
\end{aligned} \tag{4}$$

The completeness and uniqueness of this representation will be addressed below.[1]

[1] Chree (1888) and Love (1944) obtained elastic solutions in terms of spherical harmonics in spherical coordinates. Those can also be expressed in terms of polynomials in Cartesian coordinates.

These stresses are written in terms of 15 unknown constants. The three equilibrium equations can be invoked to solve for three constants, leaving 12. Then the stress boundary conditions must be imposed. On the outer surface of the ellipsoid, the tractions, given as

$$\begin{aligned} t_x &= n_x\sigma_{\mathrm{x}} + n_y\tau_{\mathrm{xy}} + n_z\tau_{\mathrm{xz}}, \\ t_y &= n_x\tau_{\mathrm{xy}} + n_y\sigma_{\mathrm{y}} + n_z\tau_{\mathrm{yz}}, \\ t_z &= n_x\tau_{\mathrm{xz}} + n_y\tau_{\mathrm{yz}} + n_z\sigma_{\mathrm{z}}, \end{aligned} \tag{5}$$

must be zero. The components of the outward normal to the external surface of an ellipsoid are given, to within an unnecessary magnitude, as

$$n_x = \frac{x}{a^2}, \quad n_y = \frac{y}{b^2}, \quad n_z = \frac{z}{c^2}, \tag{6}$$

where a, b, and c are the lengths of the principal semi-axes, always ordered from largest to smallest. Using those in the expressions (5), and using the equation for points on the surface as

$$x = a\sqrt{1 - \left(\frac{y}{b}\right)^2 - \left(\frac{z}{c}\right)^2}, \tag{7}$$

reduces each surface traction to terms that are, to within a multiple, constant, quadratic in y, or quadratic in z. Since the tractions are zero over the entire surface, each such term must be zero, a fact that can be used to eliminate nine more constants (three tractions, three terms each). The calculations are somewhat complex but straightforward and can be accomplished entirely in closed algebraic form using the symbolic algebra program MATHEMATICA.

Dobrovolskis (1982) and Slyuta and Voropaev (1997) used a similar approach to determine elastic solutions. However, they began with polynomial expressions for the displacements and then calculated the strains and then the stresses using Hooke's law, which resulted in the stress forms above. That approach implicitly assumes elastic deformation from a stress-free initial state. The approach here is to look for equilibrium stresses directly, without necessarily introducing elastic displacement considerations. Dobrovolskis (1982) also resorted to numerical methods to solve for the constants for particular application to several satellite bodies, while Slyuta and Voropaev (1997) restricted their analysis to prolate bodies without spin, where the additional symmetry allowed them to obtain closed-form solutions. In fact, the use of a modern symbolic algebra program eliminates those practical considerations.

The final form obtained for equilibrium stresses is then determined to within three final constants. That is because the general problem is statically indeterminate: the three stress equilibrium equations and the stress boundary conditions involve six unknown stresses, leaving three degrees of freedom in the solutions.

From this point, there are several ways to proceed. First, one can impose the requirement that the material is a fluid, which requires that all shear stresses be zero and the three normal stresses be equal. Doing so gives the classical hydrostatic fluid solutions. Or, one can determine an elastic solution by expressing the strains from the stresses using Hooke's law and then imposing the six strain compatibility equations. From symmetry, three of those equations are identically satisfied and the remaining three determine the last three constants and the unique elastic solution, which is exactly that given[2] by Dobrovolskis (1982). It is not repeated here. Finally, and more importantly, as per the discussion above, a different approach is used here, using the Mohr–Coloumb yield condition and limit analyses approaches.

The Mohr–Coloumb yield condition (see, for example, the soil mechanics text by Lambe and Whitman (1969)) requires that the largest (least negative and compressive here) principal stress σ_1 and the smallest (most compressive) σ_3 satisfy the inequality

$$(\sigma_1 - \sigma_3)\sqrt{1 + f^2} + f(\sigma_1 + \sigma_3) \le 2Y, \tag{8}$$

where $f = \tan(\phi)$; ϕ is the angle of internal friction (or angle of repose) and Y is the cohesion: the yield strength at zero confining pressure. In the case of zero cohesion, the friction angle required for a given stress state, in terms of the largest and smallest principal stresses, is

$$\tan(\phi) \ge \frac{\sigma_1 - \sigma_3}{2\sqrt{\sigma_1\sigma_3}} = \frac{\sigma_1/\sigma_3 - 1}{2\sqrt{\sigma_1/\sigma_3}}. \tag{9}$$

In this case, the Mohr–Coloumb envelope, in a plot of shear stress versus normal stress on any plane in the body, consists of two straight lines through the origin, as shown in Fig. 1. The slope of the lines are equal to the tangent of the friction angle. Tensile stresses are not allowed. If the friction angle is 90°, the criteria become a simple no-tension criteria with no friction effects. For any other case, if one principal stress is zero, then the other two must also be zero, since a Mohr's circle with the right side through the origin would exceed the envelope unless the least stress is also zero.

This fact can be used for points on the surface of the body. At any point on the surface on any one of the three principal ellipsoidal axes of a body, the shear stresses are zero from symmetry. The normal stress is required to be zero from the traction boundary conditions. Then that zero stress must also be the largest principal stress σ_1. As a consequence, from the observation above, the smallest principal stress must also be zero, which implies that all three principal stresses must be zero at those poles. There can be no lateral stresses. This is true whether or not those points are actually at yield, as long as the angle of friction is less than 90°.

[2] Except that closed-form solutions are obtainable using MATHEMATICA. However, since those closed-form solutions fill several pages with algebraic forms, they are not given here.

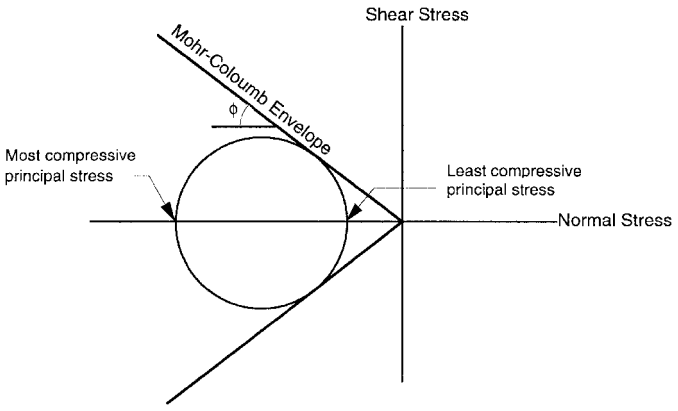

FIG. 1. A zero-cohesion Mohr–Coloumb yield function. A Mohr's circle for a stress state at yield is shown. Principal stresses in tension are not allowed. If the largest (least compressive) principal stress is zero, then the smallest must also be zero, so that the Mohr's circle for that stress state is a point at the origin.

That is, no circle through the origin can be completely inside the MC envelope unless it has zero radius.

Those conditions can then be used to determine the last three constants; the requirement is that the lateral stresses must be zero at the three poles of the body. Then, all 15 constants are determined, giving an equilibrium stress state that is everywhere within the yield criteria.

The closed-form final result for these equilibrium stresses found by this process is actually very simple; the normal stresses are given as

$$\begin{aligned}
\sigma_x &= -\rho k_x a^2 \left[1 - \left(\frac{x}{a}\right)^2 - \left(\frac{y}{b}\right)^2 - \left(\frac{z}{c}\right)^2\right], \\
\sigma_y &= -\rho k_y b^2 \left[1 - \left(\frac{x}{a}\right)^2 - \left(\frac{y}{b}\right)^2 - \left(\frac{z}{c}\right)^2\right], \\
\sigma_z &= -\rho k_z c^2 \left[1 - \left(\frac{x}{a}\right)^2 - \left(\frac{y}{b}\right)^2 - \left(\frac{z}{c}\right)^2\right]
\end{aligned} \tag{10}$$

and the three shear stresses are identically zero. Therefore the normal stresses are also the principal stresses everywhere in the body. Further, the three normal stresses are simple multiples of each other over the entire body, with the ratios depending only on the three components of the potential and the two ratios of the ellipsoidal semi-axes given as

$$\begin{aligned}
\alpha &= \frac{c}{a}, \\
\beta &= \frac{b}{a},
\end{aligned} \tag{11}$$

where always $\alpha \le \beta \le 1$. Since the ratios of the stresses are independent of position, either all points satisfy the strict inequality of Eq. (9) and are within yield or all satisfy the equality and are at yield.

For gravitational forces only, the body force potential in the form of Eq. (3) is commonly given with the three parts as

$$\begin{aligned}
k_{xG} &= \rho\pi G abc \int_0^\infty \frac{ds}{(a^2+s)\Delta}, \\
k_{yG} &= \rho\pi G abc \int_0^\infty \frac{ds}{(b^2+s)\Delta}, \\
k_{zG} &= \rho\pi G abc \int_0^\infty \frac{ds}{(c^2+s)\Delta}
\end{aligned} \tag{12}$$

with $\Delta = \sqrt{(a^2+s)(b^2+s)(c^2+s)}$. The centrifugal potential due to spin rate ω, assuming rotation about the shortest axis (always taken as z), is given as

$$V_R = -\frac{\omega^2}{2}(x^2 + y^2), \tag{13}$$

which contributes one additional term $-\omega^2/2$ to each of k_x and k_y. Finally, a tidal contribution, assuming a stable locked circular rotation about a distant parent body, has k_x, k_y, and k_z components as the coefficients of the three terms in the potential:

$$V_T = -\omega^2(x^2 - y^2/2 - z^2/2). \tag{14}$$

The total k_x, k_y, and k_z are then those in Eq. (12) plus the appropriate terms from Eqs. (13) and (14), depending on the application of interest.

The gravitational contribution can be expressed in terms of elliptical integrals in the general case, or in elementary functions for special cases, and is determined by the two ratios α and β, together with G, ρ, and a body average radius. The spin and tidal contributions depend on the rotation rate ω.

The yield condition Eq. (9) is given in terms of the ratios of the stresses; those ratios are, as noted, constant over the entire body. Consequently, the stress state is either within the yield surface at all points in the body or is just at the yield condition at all points, depending on the value of the required angle of friction given by Eq. (9) compared to the body's actual angle of friction. Conditions exceeding the yield condition are not allowed. Therefore the required angle of friction for a given body to be in the equilibrium state above is determined solely by α and β and the spin rate ω. If the body yields at any one point, it will do so also at all other points.

3. UNIQENESS OF EQUILIBRIUM STATES, LIMIT SOLUTIONS, DEFORMATION, AND STABILITY

The linear elastic solution from a stress-free initial state, which is contained in the forms (4) assumed above, is known to be unique to within a rigid body motion. Therefore, the starting forms (4) are sufficiently general to recover that solution. However, for a general elastic–plastic problem, only the increments (or rates) of stress, strain, and displacement are unique, and final solutions for a particular loading history characteristically have discontinuities in the slopes when plotted as a function of the coordinates. (See, for example, Fig. S5.25 in the text by Chen and Zhang (1991).) Those solutions are certainly in equilibrium, so it is obvious that the smooth starting forms (4) cannot possibly contain all equilibrium solutions to the general elastic–plastic problem. However, limit solutions are generally smooth, and those are the goal here. It is shown next that the above solutions, as limit solutions, are also unique.

Chen and Han (1988) discuss the limit load approach. A "limit load" or "collapse load" for a body is defined as a load state for which the plastic deformation can increase without limit in the body. If the body has several types of loads (e.g., gravitational and spin) then it is convenient to let all increase from zero with some common scale factor μ and seek the value $\mu = \mu_0$ where collapse occurs. Since the elastic strains play no role in the collapse state, those elastic effects can be ignored in the analysis (Chen and Han 1988, p. 414).

As a consequence, the analysis proceeds assuming a rigid-plastic material, for which the elastic strains are all zero. Then the plastic strain rates are assumed to be given by a flow rule of the form

$$\dot{\varepsilon}_{ij} = \dot{\lambda}\frac{\partial g}{\partial \sigma_{ij}}, \tag{15}$$

where g, the so-called plastic potential, is some function of the stresses, and $\dot{\lambda}$ is some positive scalar factor of proportionality. Commonly, the plastic potential g is assumed to be the same as the yield function f, and the flow rule is called "associated." Then Eq. (15) implies that the strain rate vector is perpendicular to the yield surface in stress space.

Here the Mohr–Coloumb yield condition is used. Chen and Han (1988) give the explicit form of the associated flow rule for that case. The result depends on which principal stress is largest and which is smallest. Suppose that the numbering of the principal stresses is always from the largest to the smallest. Then, assuming all three are distinct, the flow rule for the three strain rates is given as

$$[\dot{\varepsilon}_1 \quad \dot{\varepsilon}_2 \quad \dot{\varepsilon}_3] = \dot{\lambda}[m \quad 0 \quad -1], \tag{16}$$

where the constant m is related to the angle of friction:

$$m = \frac{1+\sin\phi}{1-\sin\phi}. \tag{17}$$

Note that since the shear stresses are zero, these strain rates are also the x, y, and z components, in some order. When two of the stresses are equal, the stress point is at a corner on the yield surface and the strain rates are indefinite but are always a sum of two terms similar to Eq. (16) (see Chen and Han 1988). That special case is not considered in detail here.

For fairly general yield functions and flow rules, and specifically for this one, there are two limit theorems that form the basis of limit analysis. The first uses the definition of a *statically admissible stress field*: it is any stress field that satisfies the equilibrium equations and the stress boundary conditions and nowhere violates the yield condition. The solution above is statically admissible whenever it satisfies Eq. (9). Then the first (lower limit) theorem states that the loads associated with that stress field are less than or equal to the actual limit load. Therefore the loads (spin and gravitational) that equate to yield Eq. (9), used in the stress state given in Eq. (10), are necessarily less than or equal to the collapse load. Thus, those loads are a *lower limit* to the collapse loads.

Secondly, a *kinematically admissible velocity field* is any velocity field leading to unconstrained flow (collapse) that satisfies the given velocity boundary conditions (of which there are none in the present problem). Hence here any choice of a collapse velocity field, and its corresponding strain rates, gives a kinematically admissible velocity field. The second (upper bound) theorem states that the loads associated with any such velocity field are greater than or equal to the actual collapse load. (Actually the form in Chen and Han (1988) refers to the rate of dissipation, which is related to the loads.)

It is useful to quote the paraphrasing of these two limit theorems as given by Chen and Han. They state, "The lower bound theorem expresses the ability of the ideal body to adjust itself to carry the applied loads if at all possible." For the second, upper bound, result they state, "If a path of failure exists, the body will not stand up."

If a velocity field that is derived from the statically admissible solution is also kinematically admissible, then that kinematically admissible velocity field has the *same* loads as the statically admissible stresses, the upper and lower load limits coincide, and those loads are indeed the actual limit loads. That same result is also expressed in a different way by a result given by Chakrabarty (1987, p. 96), where he proves that: "the state of stress at the yield point is uniquely defined in a region where the material can deform under given boundary conditions." The "can deform" proviso is the same as the existence of the kinematically admissible collapse state. His definition of the "yield point" refers to that of the *body* and is the same as the limit load.

Therefore, to prove the uniqueness of the stresses above as those at the limit load of the body, we noted already that they are simultaneously at the yield point for all locations in the body, if the loads are derived by using Eq. (9) with the equality. Their associated strain rates can then be calculated from the flow rule, Eq. (16). Those can be used to get a velocity field.

Let the coordinate axes be relabeled as x_1, x_2, x_3 to correspond to the ordering of the principal stress axes, that is, order x, y, and z depending on which axes have the largest, intermediate, and smallest principal stress. Then the velocity field in this reordered coordinate system can be taken as

$$v_1 = x_1 m\dot{\lambda}, \quad v_2 = 0, \quad v_3 = -x_3\dot{\lambda}, \tag{18}$$

which is a uniform stretching: an expansion along the direction of the first axis, a shortening along the third, and no motion in the direction of the second. The strain rates from Eq. (18) are then those of the flow rule Eq. (16). The magnitude of the scalar $\dot{\lambda}$ is indeterminate, but positive, which is a usual feature of plasticity without hardening. It might be noted that there is a volume expansion (the sum of the three) associated with this motion, since $m \geq 1$ for all angles of friction. That volume expansion is a consequence of the fact that the flow rule associated with the Mohr–Coloumb yield function has a dilation component.[3]

Then this is the sought after, kinematically admissible velocity field. Its existence and its derivation from the stress field proves that the form Eq. (10) with the loads giving the yield function (9) with the actual angle of friction is the unique stress field at the limit load for that angle of friction. Those loads are the limit loads for that angle of friction. These results also justify the starting forms (4), i.e., those initial forms are sufficiently general to include both the elastic solution and the elastic–plastic limit load solution, although they do not include many possible equilibrium states with intermediate yielding and flow.

The flow rule also gives important additional information. When a body yields at loads corresponding to its angle of friction, the flow rule (16) predicts a change of shape. The change of shape would also give a change in the spin rate, conserving the angular momentum. If that change moves toward a new shape that is in equilibrium for a smaller angle of friction, then the deformation can be considered to be stable. Otherwise the new configuration requires a larger angle of friction, and the deformation would be expected to proceed in an unstable manner at an increasing rate, leading to disruption of the body. While the general question of stability is not addressed here, such a consideration is made below for Phobos.

4. REQUIRED ANGLE OF FRICTION

To obtain results, a specific angle of friction is chosen, and Eq. (9) is used with the equality to solve for the limit load. It is useful to express the solutions in nondimensional form. The two aspect ratios α and β of the ellipsoidal principal axes have already been introduced. The three scaled coordinates can be given in terms of ratios of the coordinates to their respective semi-axes lengths. An equivalent-volume average radius is defined as $R = (abc)^{1/3}$. Any stress component can be scaled as

$$\bar{\sigma}_i = \frac{\sigma_i}{\rho^2 G R^2} \tag{19}$$

and a scaled spin rate is conveniently defined as

$$\Omega = \frac{\omega}{\sqrt{\rho G}}. \tag{20}$$

The *ratio* of any two stresses is then independent of size scale R. Then, since Eq. (9) has only stress ratios, the required friction angle is expressible in terms of only α, β, and the scaled spin Ω and is independent of the asteroid size. The only complication is that in various cases one must determine which stress component is the maximum and which is the minimum. Then, for each α, β, and Ω, one can determine a value for the required friction angle. To get two-dimensional plots, contour curves for the required angle ϕ are shown on a plot of α versus Ω for some given value or relation for β. Those also give, for that choice of β, the limits of the aspect ratio α for a given Ω, i.e., limit shapes for a given spin state.

Note that the solutions here are unique only as *limit loads*. That is, a stress state on a contour curve for, say, $\phi = 10^\circ$ is not the only equilibrium stress state for a material with actual angle of friction $\phi = 30^\circ$. Many other equilibrium states are possible. It is, however, *the unique limit load* if the material has the actual angle of friction $\phi = 10^\circ$: then any larger loads would give unconstrained plastic deformation.

Also it should be noted that the limit solutions are for ideal smooth ellipsoidal shapes, and all points are just at the MC yield condition. It is not necessary to have surfaces with slopes for the stress state to be at the MC limit. If in fact surface features and slopes are to be allowed, then the body must be clearly within the smooth shape limit, so that the perturbations in the stress field due to those features still results in a stress state within yield.

Special cases follow.

4.1. Oblate Spheroids

The first case presented is for oblate spheroids, with $b = a$ and therefore $\beta = 1$. There are assumed to be gravitational forces and arbitrary spin rate but no tidal forces. The contour curves of required friction angle are as shown in Fig. 2.

Certain aspects of this figure are worth noting. First, the upper curve is an overall limit case, with the friction angle of 90° and $f = \tan(\phi) \to \infty$. This is a spin limit at which k_x becomes zero: the spin is sufficient so that the x component of body force becomes zero at all locations in the body. For any higher spin rate the entire body would require tensile stress in the x direction, which it cannot withstand. The intercept at the top right for the spherical case with $\alpha = 1$ is at the scaled spin $\Omega = \omega/\sqrt{\rho G} = 2\sqrt{\pi/3} \approx 2.05$. This is the limit given by Harris (1996) for spherical bodies; he simply equated the centrifugal acceleration to the gravitational acceleration at the equator. It is then an upper bound for all ellipsoidal bodies. If the mass

[3] Lambe and Whitman (1969, p. 129) discuss such behavior in dry sands.

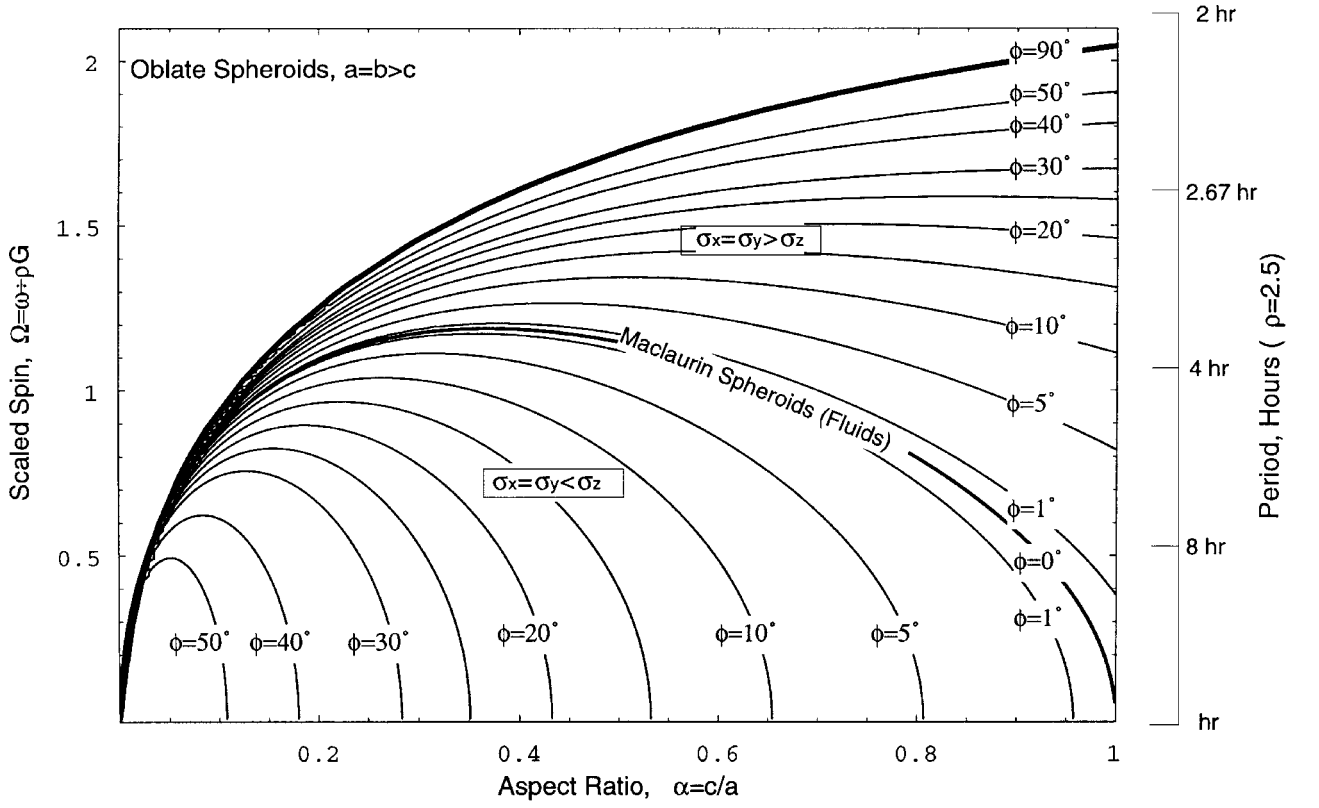

FIG. 2. Required angle of friction for oblate spheroids with spin. The Maclaurin spheroids on the central curve are for fluid bodies with zero angle of friction. For any nonzero angle of friction there is a region of equilibrium spins bounded by an upper curve of maximum spin and a lower curve of minimum spin rate. Equally, for a given spin, there is a left limit of maximum possible eccentricity and a right limit of minimum eccentricity. For a given friction angle, states between the two limit curves are permissible equilibrium states.

density is assumed to have the generic value $\rho = 2.5$, that limit corresponds to a period of 2.1 hr. Harris (1996) further assumes that, for nonspherical cases, this value decreases linearly to zero with the aspect ratio α; the actual curve as shown on the figure is not linear.

It is seen that for common angle of friction values for soils (typically about 30°) this universal limit cannot be reached; it is about 25% too large for near-spherical bodies. For that angle of friction and for a spherical body the maximum spin, assuming a generic value of 2.5 again for the mass density, has the period of 2.56 hr, about 20% slower. If the mass density is ρ is 1.5, then the maximum spin rate allowed at that friction angle has the period of 3.3 hr. Also, nonspherical bodies with that friction angle have essentially the same permissible spin values for any moderate nonsphericity; i.e., the larger friction angle curves are almost flat for $0.3 \leq \alpha \leq 1$.

All states on this plot have $\sigma_y = \sigma_x$ as required by geometrical symmetry and the fact that the rotation is about the z axis. When the angle of friction is zero, as for a fluid, it is also required that $\sigma_z = \sigma_y = \sigma_x$. The curve of those states is in the center of all curves and gives the locus of the *Maclaurin spheroids*. For spin rates less than those on that Maclaurin curve, the stresses σ_x and σ_y are less than σ_z (more compressive), and increasing spin offsets the gravitational stresses in the x and y directions. Therefore the required angle of friction *decreases* with increasing spin rates. Above the Maclaurin curve, the required angle of friction *increases* for increasing spin rates. For each given angle of friction ϕ there are then two limit curves, one below and one above the Maclaurin spheroid curve. Any state between those two curves requires *less* angle of friction than ϕ, so that it is a possible equilibrium state for that angle of friction ϕ, and the stress states from Eq. (10) are everywhere within yield.

When a state is on a limit curve for some given friction angle, and subsequently yields, the velocity field (17) gives the deformation rates. For states below the Maclaurin curve, yield could be induced, for example, by decreased spin from some external mechanism. In this region the x and y stresses are smaller than the z stress, so that the z stress is σ_1. Then the velocity field has a uniform expansion in the shortest z direction and a contraction in either the x or y direction, which can be taken to be equal. This is a simple shape change toward more sphericity as the spin is reduced. Offsetting that, the decreased elongation and balance of angular momentum tend to increase the spin again. Whether the net effect is a decreased required friction angle or an increased one is not determined here in the general case. If it is increased, this is an indication of an unstable deformation.

For states above the Maclaurin curve, where the spin is greater than that allowable in a fluid body at that same shape, the equal x and y stresses are greater than the z stress. Then the z stress is σ_3, and the velocity field leads to an increased oblateness when yielding occurs.

4.2. Prolate Spheroids

This case has the intermediate axis length b equal to the shortest one, $b = c$, so that $\beta = \alpha$. In this case all three normal stresses can be different, and in different regimes different ones determine the yield condition. The contour curves for constant friction angle are given in Fig. 3.

The states below the curve labeled $\sigma_z = \sigma_x$ have $\sigma_x < \sigma_z < \sigma_y$. In that lower region, increasing spin rate decreases the required angle of friction. Just above that curve there is a central region with $\sigma_z < \sigma_x < \sigma_y$ and increasing spin rate requires increased angle of friction. Above the next curve labeled $\sigma_y = \sigma_x$, $\sigma_z < \sigma_y < \sigma_x$ and increasing spin rate still requires increased angle of friction. For these prolate spheroids, the only fluid solution with $\phi = 0$ must have zero spin and the body must be spherical, at the lower right point of the plot. For the angle of friction of 5° there is a possible region at the lower right and another toward the left in the central region where $\sigma_z < \sigma_x < \sigma_y$. For the cases of $\phi = 5.5°$ or more, the possible states are bounded by a lower curve and an upper curve, as in the previous oblate cases. Any state between those two limit curves are possible without yield. The upper overall limit case is again where the x body force becomes zero, and further spin would require tensile x stresses.

4.3. Intermediate Ellipsoids

A case that is intermediate to those two just given has the ellipsoidal intermediate axis length equal to the average of the largest and smallest: $b = (a + c)/2$. The contour curves in this case are shown in Fig. 4.

In this case there are six distinct regions, as labeled with different combinations of stress inequality values, bounded by three curves where two stresses are equal. There is a single point where all three stresses are equal, which is the *Jacobi ellipsoid* for this case; it has $\alpha = 0.498$, $\beta = (0.498 + 1)/2 = 0.749$, and $\Omega = 1.0663$. For very small angles of friction, there are two distinct regions of permissible states. For any fixed ϕ greater than about 2°; there is a single region bounded again by an upper curve for a maximum spin rate and a lower curve giving a minimum spin rate. Any state between those two limits requires less angle of friction and is therefore a permissible equilibrium state for a given angle of friction. Note that the regions include points at smaller aspect ratio c/a (to the left) than the Jacobi ellipsoid: those ellipsoids do not furnish a lower limit to the aspect ratio. Also, it is not necessary for the shapes of rubble-pile asteroids to lie close to the Jacobi point; significant deviations are possible.

All three plots have the same intercepts at the right axis for spherical bodies, but the upper overall limit and limits for particular friction angles are distinct depending on the magnitude of the intermediate aspect ratio β.

5. ASTEROID SHAPES AND SPINS

We can now compare the observations of asteroids to the equilibrium shape limits derived here, with the hope of gleaning information or constraints on their internal structure and material. The compilation of asteroid periods and lightcurve amplitudes given by A. Harris and P. Pravec were obtained from Alan Harris (personal communication). Following the lead of Pravec and Harris (2000), a list of near-Earth asteroids, Mars-crossers, and main belt asteroids was generated; Trojans and Centaurs were excluded. That left 845 asteroids. It was assumed that the largest observed full-range amplitude of lightcurve variation in magnitudes was due solely to the difference between the largest and intermediate diameter, so that the usual relation for the amplitude

$$A = 2.5 \log\left(\frac{a}{b}\right) \tag{21}$$

was used to determine the aspect ratio $\beta = b/a$. While it is well known that this equation may not be entirely reliable, it is assumed here to give a good estimate of the shape. No attempt to assign a minimum axis c was made; instead the data are shown on plots of various plausible c values. In particular, since $c \le b \le a$, we have also $\alpha \le \beta \le 1$ and then, for any given β, α can take on any lesser value. Thus in this case it is useful to generate plots where $\alpha = k\beta$ and k can range from 0 to 1. Figure 3 above has $\beta = \alpha$, so that $k = 1$, which is the upper limit on axis c. Another popular assumption (with minimal justification) is that $\alpha = 1/2$ and $\beta = 1/\sqrt{2}$, so that $k = 1/\sqrt{2}$. Therefore further plots are generated for that case, as discussed below.

5.1. The Asteroids Assuming Prolate Spheroids: $\alpha = \beta$

These limit curves were already presented above. The data for asteroids can then be superimposed on the previous limit curves. The data for all with quality $Q \ge 2$ (see Harris 1996 for definition) are used on all plots.

For the *C-type* asteroids, on Fig. 5, a mass density of 1.5 g/cm^3 was used to calculate the scaled spin rate $\Omega = \omega/\sqrt{\rho G}$. For the C-types, those with the better quality, $Q \ge 3$, are depicted with circles around the points. There are a total of 120 data points, and 51 with $Q \ge 3$. All these C-types easily fall within friction angle limits typical of dry soils, which typically are in the range of 30°–40° even for relatively loose packing. Indeed, all of them fall within the 15° limits except for 725 Amanda on the upper 25° curve. However, one notable exception not shown is the newly discovered fast spinning asteroid 1998 KY26, with an apparent aspect ratio of 0.76 and a scaled spin rate of about 30, about 15 times higher than the limits of this curve. It is clearly not a rubble-pile asteroid.

For S-type asteroids, a mass density of 3.0 was used. If they are silicate minerals but rubble piles, a density of about *2* might

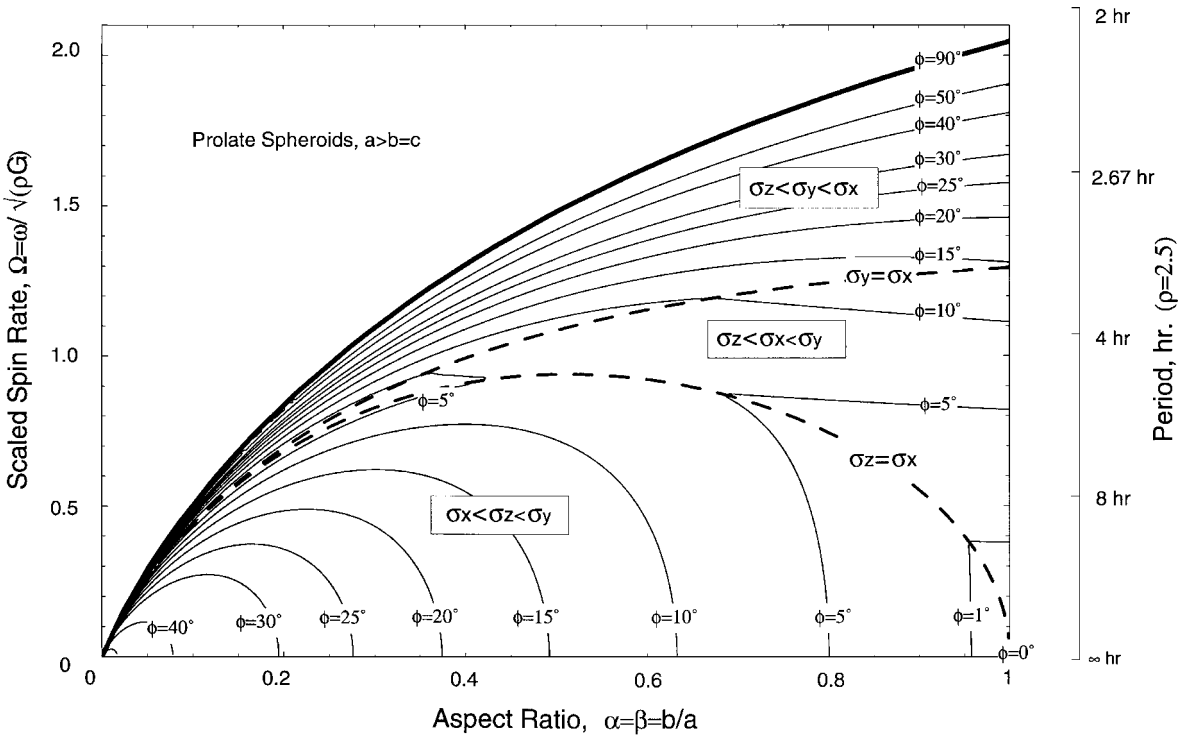

FIG. 3. Required angle of friction for prolate spheroids with spin. For any nonzero angle of friction there is a region of equilibrium shapes. No nonspherical fluid possibility with spin exists here.

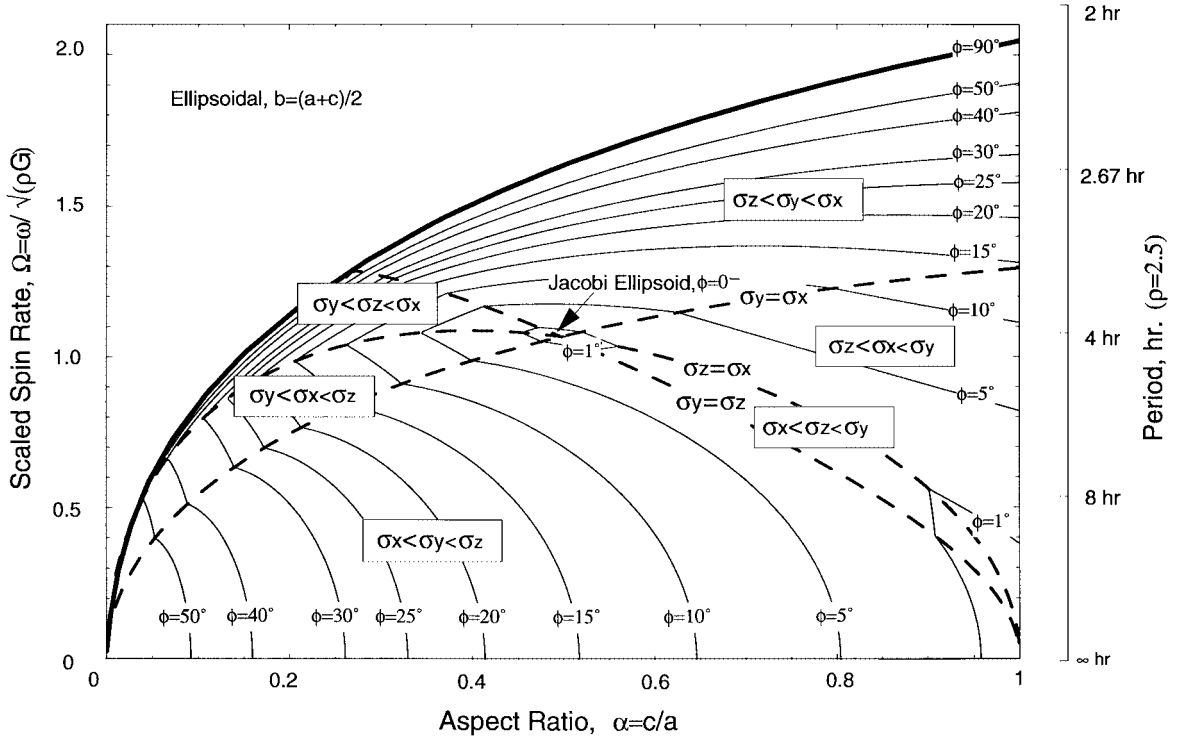

FIG. 4. Required angle of friction for ellipsoids with $b = (a + c)/2$ with spin. One Jacobi ellipsoid point exists at the center, for a fluid body with zero angle of friction. For any nonzero angle of friction there is a region of equilibrium shapes, bounded by a lower curve of minimum spin and an upper curve of maximum spin.

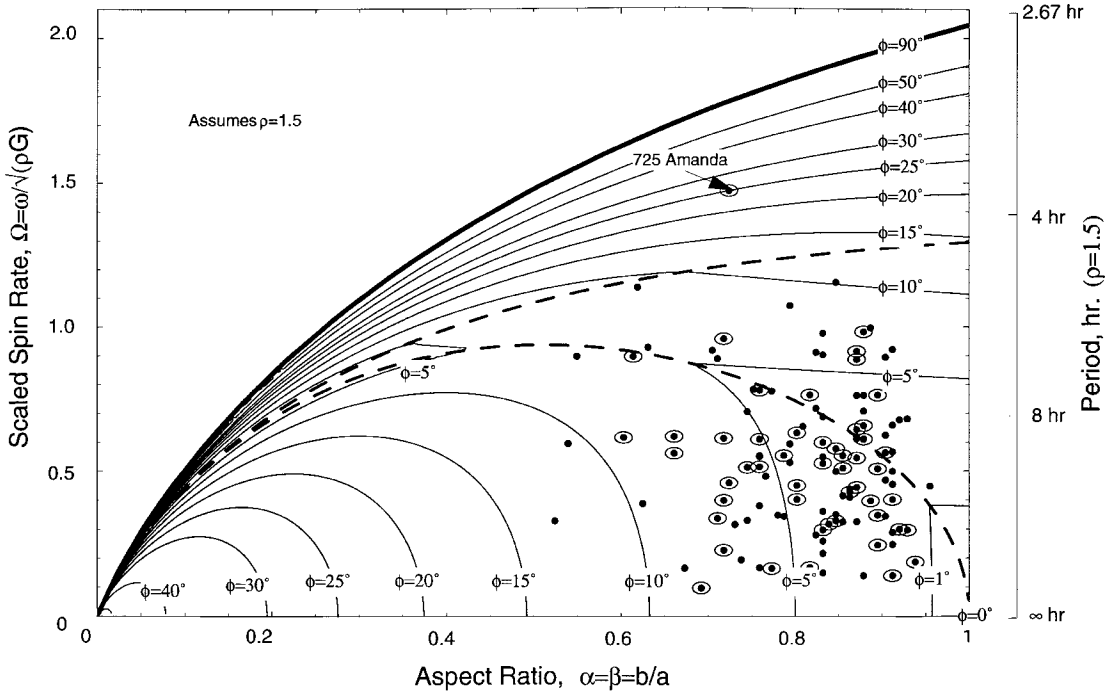

FIG. 5. Shapes and spins for C-type asteroids, compared to limit curves, assuming prolate asteroid shapes, $c = b$. Only three asteroid points lie outside the limits for $\phi = 10°$.

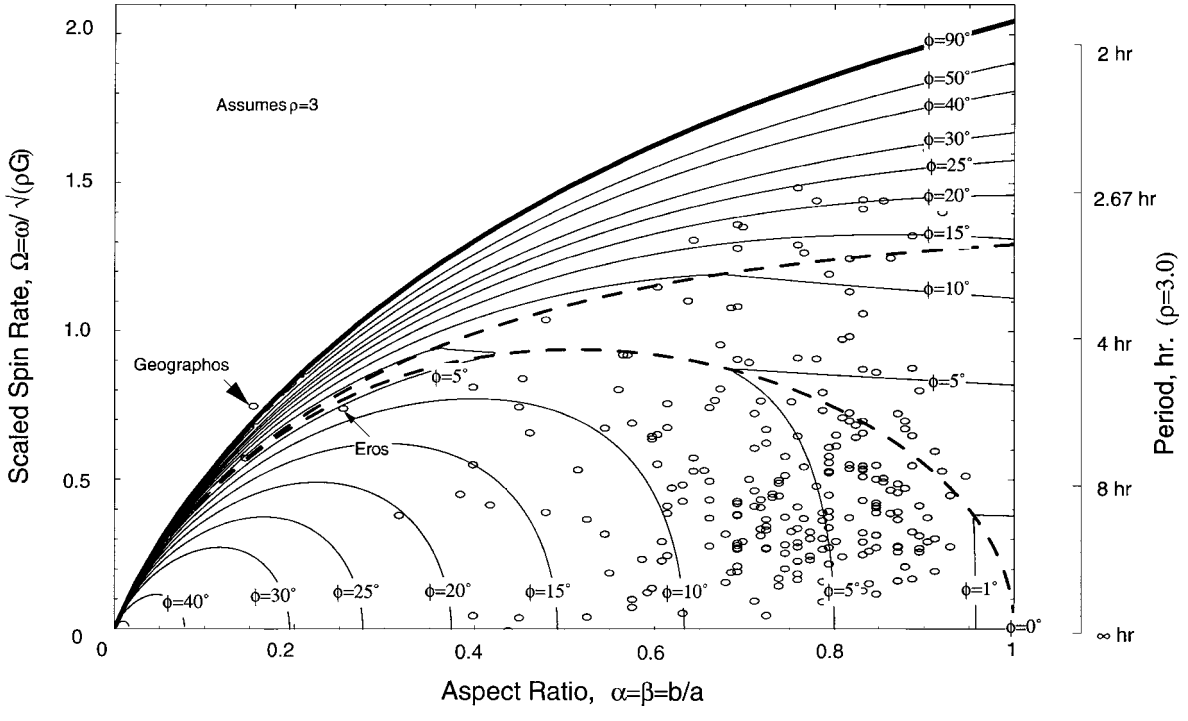

FIG. 6. Shapes and spins for S-Type asteroids, compared to limit curves, assuming prolate shapes, $c = b$. Only 1620 Geographos is outside the curves for a 25° friction angle, although about a 30% increase in its assumed aspect ratio b/a would put in within those curves.

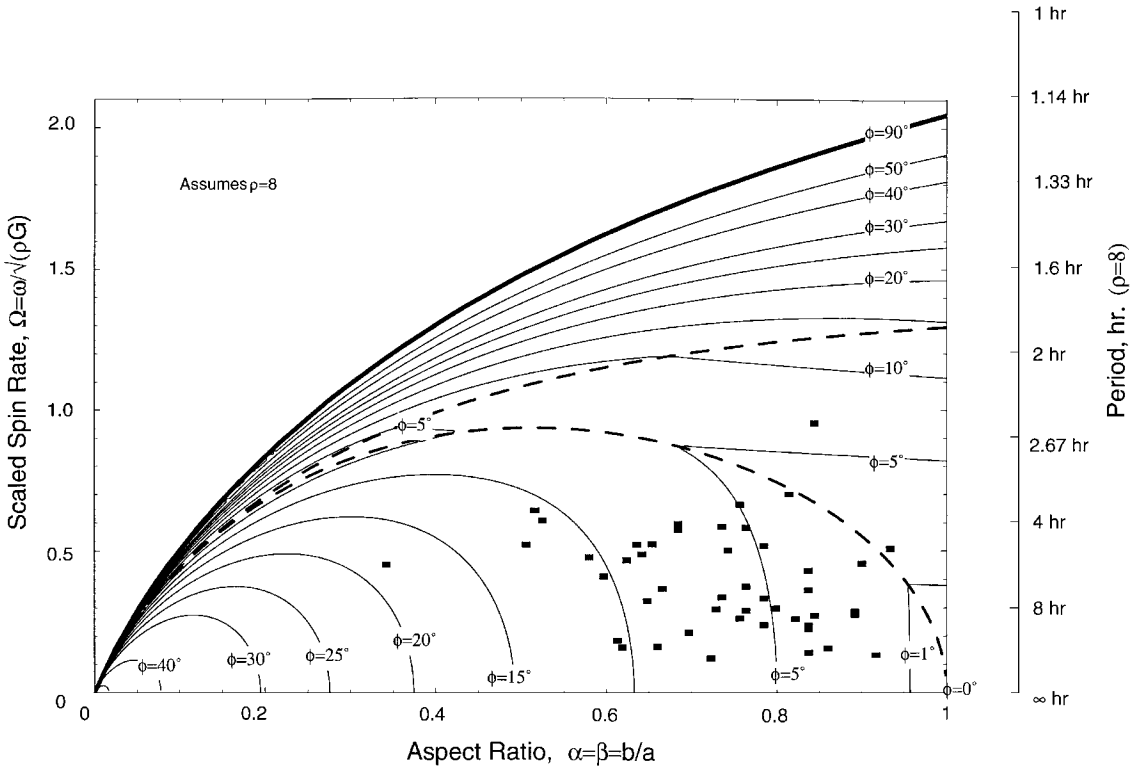

FIG. 7. Shapes and spins for M-Type asteroids, compared to limit curves, assuming prolate shapes, $c = b$. All points lie inside the limits for $\phi = 20°$.

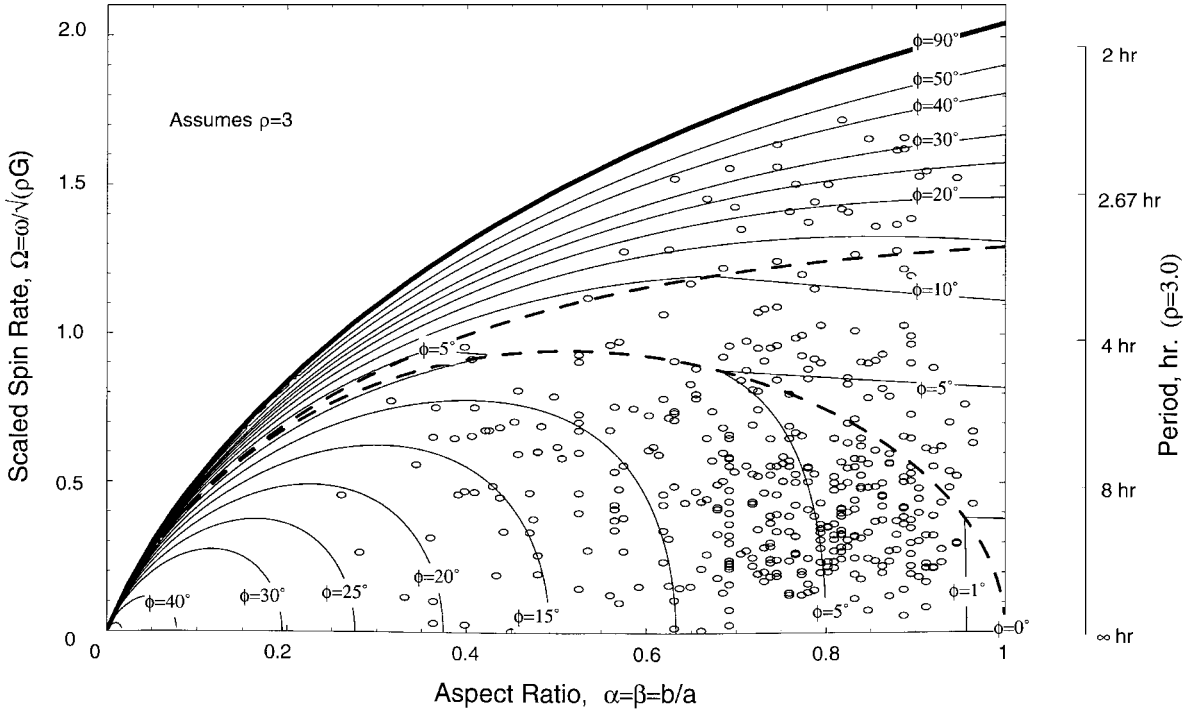

FIG. 8. Shapes and spins for all other asteroids, compared to limit curves, assuming prolate shapes, $c = b$. All points lie inside the limits for about $\phi = 42°$.

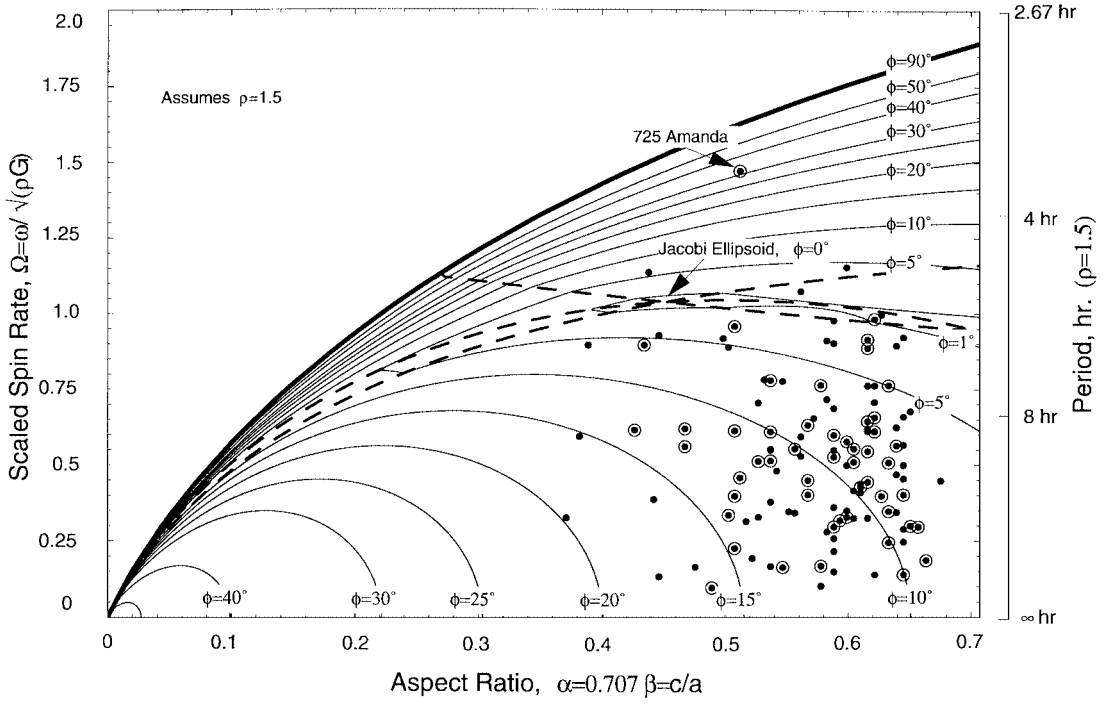

FIG. 9. The limits compared to data for spin rates and shapes of asteroids of the C-type, assuming that the smallest axis c is 0.707 times the intermediate axis b. Only one asteroid, 725 Amanda, has a state outside the limits for $\phi = 20°$, and most are within the limits for $\phi = 15°$.

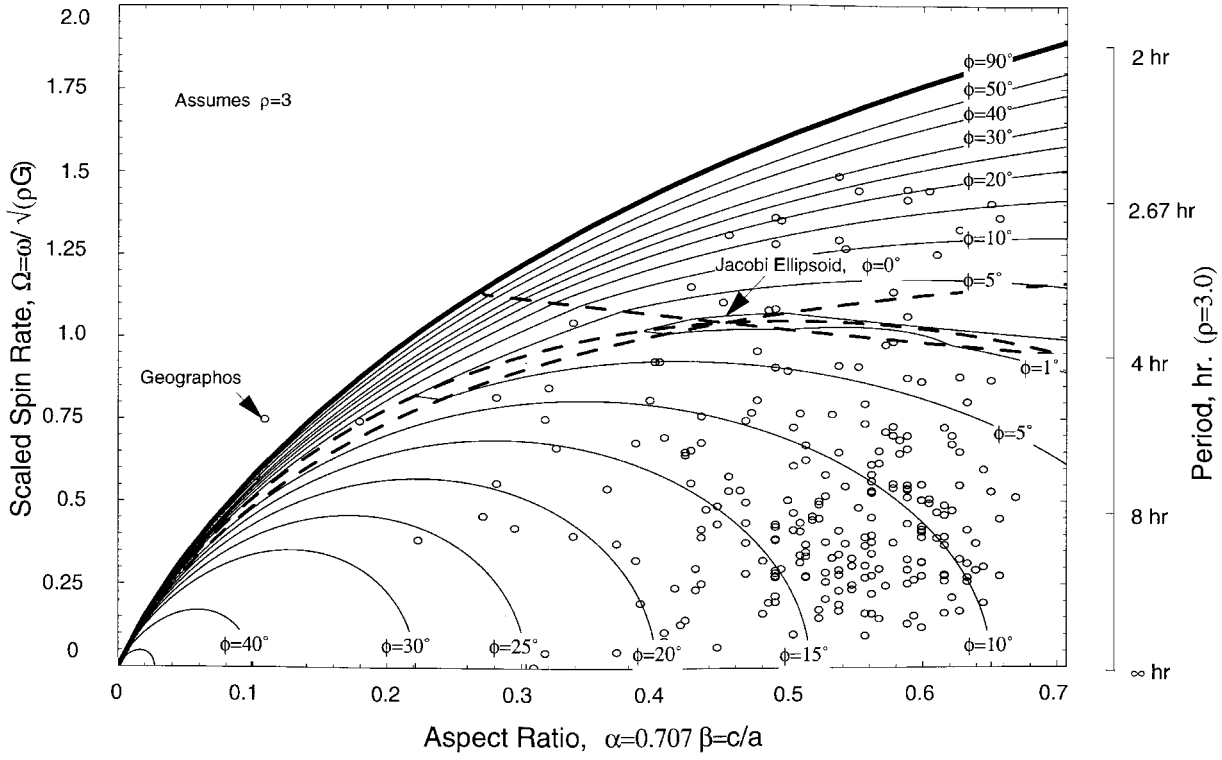

FIG. 10. The limits compared to data for spin rates and shapes of asteroids of the S-type, assuming that the smallest axis c is 0.707 times the intermediate axis b. Only 1620 Geographos at the left is essentially outside the limits for a rubble-pile structure with 30° friction angle, a result of its highly elongated shape.

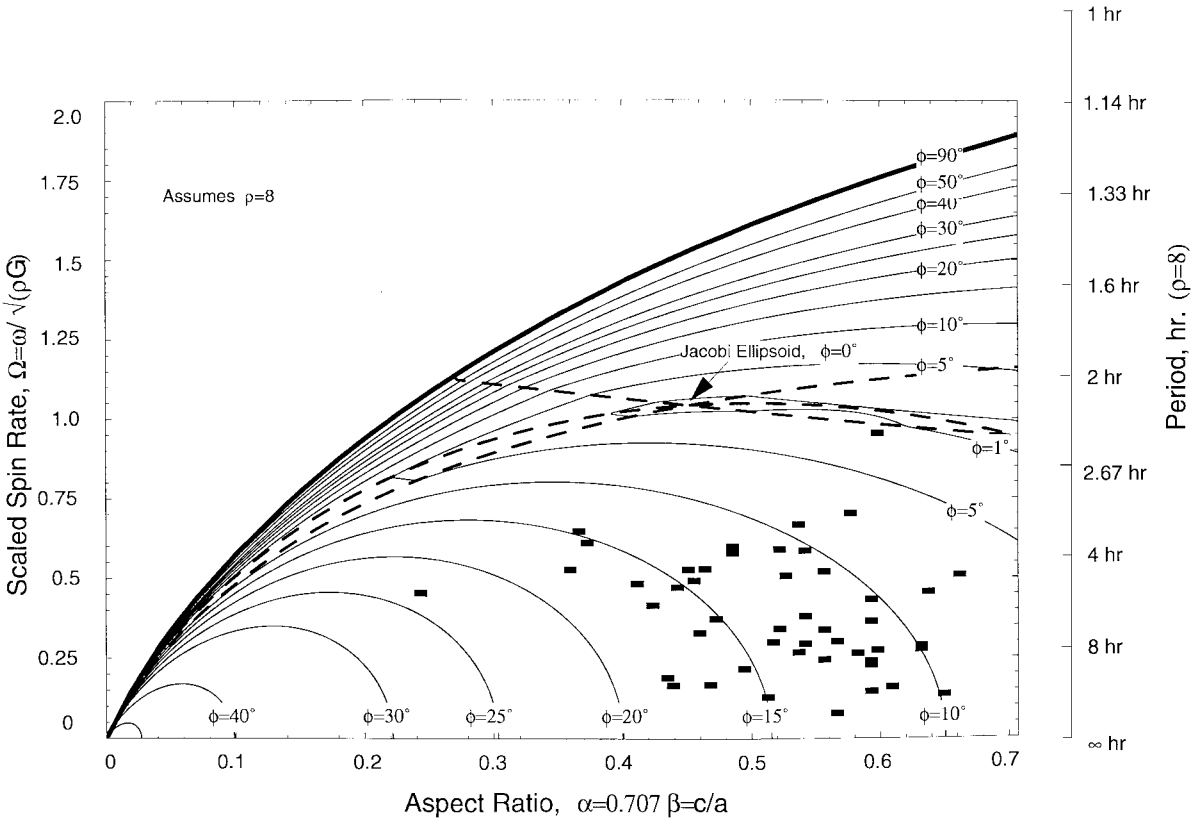

FIG. 11. The limits compared to data for spin rates and shapes of asteroids of the M-type, assuming that the smallest axis c is 0.707 times the intermediate axis b. All are within the limits for a 20° angle, and all are below the fluid case.

be more appropriate, which would raise all points by about 25%. There are 246 data points, as shown on Fig. 6. Two, Eros and 1620 Geographos, are noted. Geographos is the only asteroid outside the 20°–25° friction angle curves; however, it would plot within the curves if its ratio of intermediate to longest axis were only about 20% greater. Eros requires only a 5° friction angle to be a rubble-pile asteroid, although it is now thought that it is not a rubble-pile asteroid.

The data for M-types include 49 asteroids. While it may be less likely that a rubble-pile structure is appropriate for those, it is interesting to plot them anyway. A mass density of 8.0 was used for all points, although if they are predominantly iron but have porosity, a more appropriate value would be on the order of 5, which would increase the scaled spin by a factor of about 25%. The data are in Fig. 7. Note that all except one are near the lower branch limits.

Finally, there remain 426 other cases. A mass density of 3.0 was used for all; they are shown in Fig. 8. Only 3 fall outside the 35° limit curve.

5.2. *The Asteroids with* $\alpha = \beta/\sqrt{2}$

For $k = 1/\sqrt{2}$, the values of α are diminished from the β values determined by the lightcurve magnitudes by that ratio, and so, compared to the case above, all data points move to smaller α values. The maximum β is 1, and so the maximum $\alpha = 0.707$, which gives a new range for the plots. Figure 9 shows all C-type asteroids with quality $Q > 2$; those with $Q \geq 3$ are enclosed in circles.

The S-types are as in Fig. 10. Only one (1620 Geographos) is outside the 30° curves, but again a relatively small increase in its aspect ratio α value would put in within the curves.

The data for the M-types are in Fig. 11, and all others are shown in Fig. 12. Only in the latter case are any outside typical values for the friction angle, and none require tension.

6. AN APPLICATION TO PHOBOS

Dobrovolskis (1982) applied his elastic solution to Phobos. The parameters for Phobos are taken as

$$a = 13{,}300\,\text{m},$$
$$b = 11{,}000\,\text{m},$$
$$c = 9{,}200\,\text{m},$$
$$\omega = 2.28 \times 10^{-4}\,\text{rad/s},$$
$$\rho = 2.2\,\text{g/cm}^3$$

and it is assumed to be in a circular orbit at 2.76 Mars radii. At the center, he reported the pressure to be "about 700 mbar" (the exact elastic solution is actually 694 mbar).

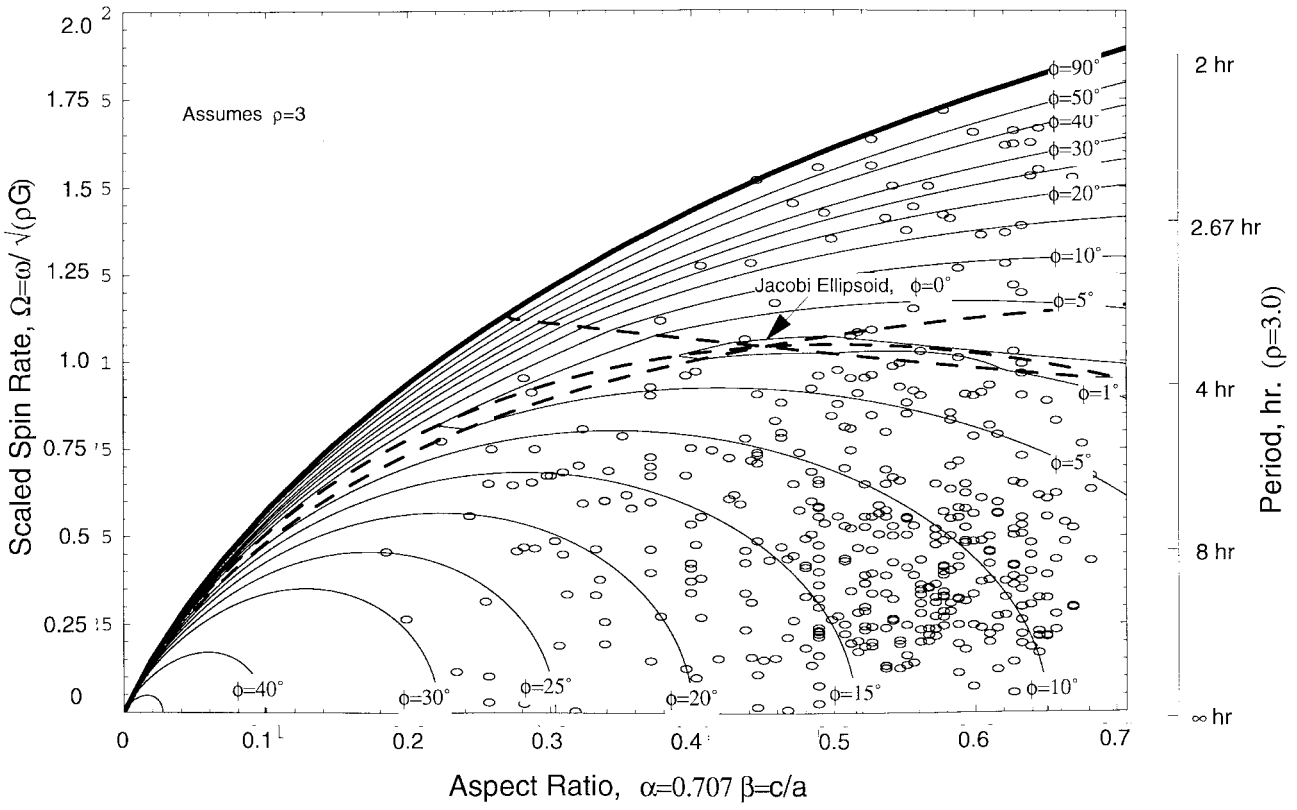

FIG. 12. The limits compared to data for spin rates and shapes of asteroids of all other types, assuming that the smallest axis c is 0.707 times the intermediate axis b. Very few are above the limits for typical values for the angle of friction, and none require tension (above the 90° curve).

In fact, if Phobos is a zero-cohesion Mohr–Coloumb body, then the elastic solution cannot be valid. Every elastic solution has lateral stresses at the surface, which, according to the analysis above, cannot be true here unless the friction angle is 90°. However, Dobrovolskis notes that only a small cohesion would be required at the surface from the elastic solution.

The stresses here in the inelastic solution are not significantly different, but note that the states here are not unique except as a limit case. Using all of the same data for Phobos, we find that the pressure at the center of this inelastic solution is 732 mbar, and all three normal stresses are roughly equal. The maximum shear stress at the center is 89 mbar, compared to the 74 mbar of the elastic solution. Obviously, both solutions are close to a pure fluid hydrostatic solution, which is determined by statics alone. However, failure considerations are different here. Among other things, the stresses in the present solution do not require cohension at the surface.

Figure 13 shows the envelopes of required friction angle for bodies when the tidal forces of a locked rotation around a parent body are included in the gravitational and spin body forces. It is otherwise for the same case given above, where the intermediate axis b is the average of the largest and smallest: $b = (a + c)/2$. Since Phobos very nearly satifies that relation, this is the convenient plot to show its state on. Its spin rate of 2.28×10^{-4} radians per second gives the scaled spin value of 0.595. The ratio of smallest to largest axis is 0.69. That point is shown on the curve; it requires a friction angle of only 7.4°. It is unlikely that Phobos is presently at a limit case dictated by strength considerations. Further, assuming a typical friction angle of 30°, it is clearly nowhere near a *tidal limit* for a MC body, although it may be at the (fluid) Roche limit depending on the exact value for its density.

Dobrovolskis (1982) considers the fate of Phobos as it approaches closer to Mars over the next $\sim 10^8$ years and its rotation rate increases. He notes that at a distance of 1.9 Mars radii, surface gravity will vanish at the sub- and anti-Mars points and loose material would be lost.[4] He shows the elastic solution stresses at a scaled distance of 2.0 radii.

Figure 14 shows the cross-plot of required angle of friction as a function of orbit distance from the present analysis. For the inelastic solution, assuming a typical friction angle of 30°, the closest possible approach in the present configuration is 2.12 Mars radii, greater than given by Dobrovolskis. The spin rate at that distance, assuming it is still locked, is $\omega = 3.383 \times 10^{-4}$ rad/s. The nature of the yield deformation can be determined here by using the velocity field given in Eq. (18). The state of Phobos

[4] In fact, if it truly has zero cohesion, it could not have the elastic solution at its present distance.

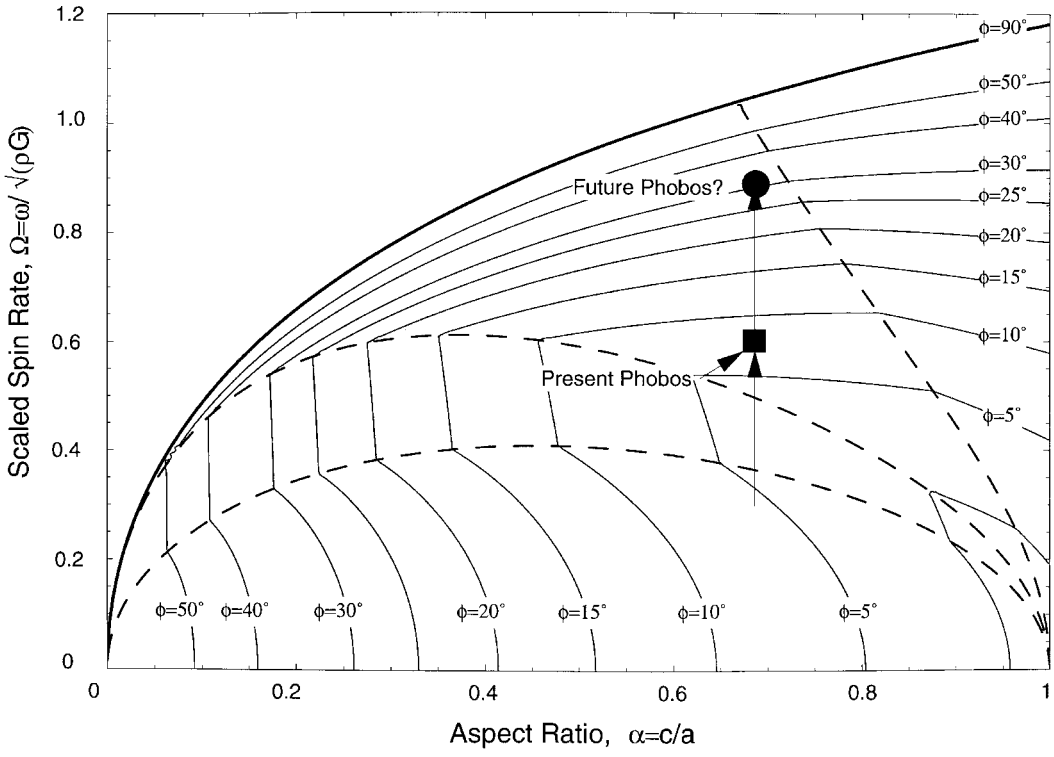

FIG. 13. Envelopes of required friction angle when locked rotation tidal forces are added to the gravitational and spin forces, for the case where the intermediate axis is the average of the largest and smallest, $b = (a + c)/2$. The data point shows the present configuration of Phobos. The arrow shows the increasing rotation rate states as it approaches more closely to Mars over the next $\sim 10^8$ years. If it is a rubble pile with a friction angle of 30° then at the top of the vertical arrow, equilibrium is no longer possible. The detailed results from the flow rule show that an increasing value of friction is required for the plastic deformation, indicating a global catastrophic disruption with an unconstrained expansion along its longest axis.

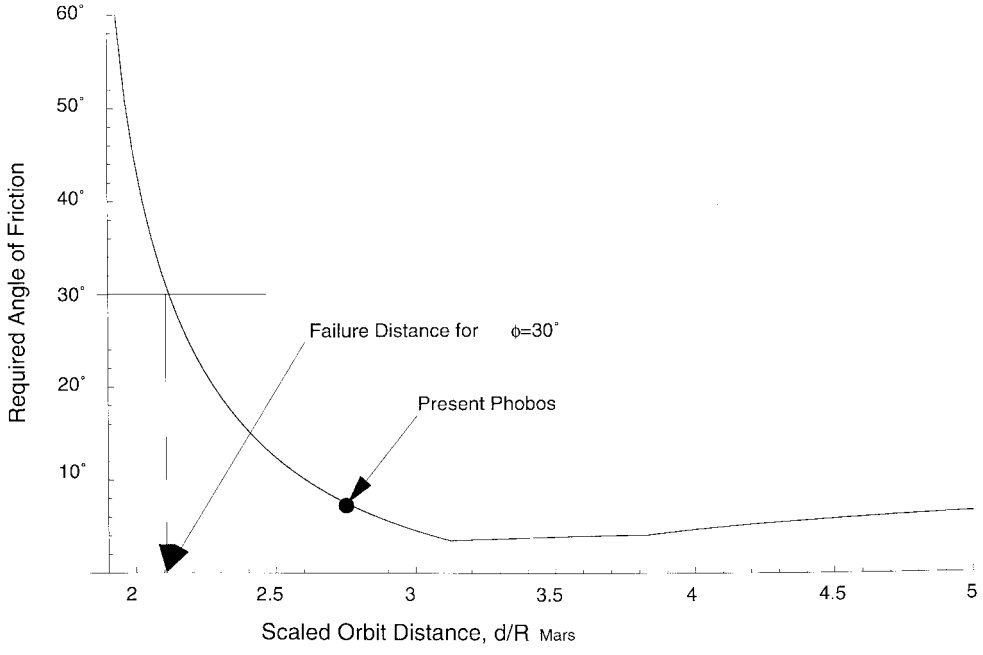

FIG. 14. The required angle of friction for equilibrium of Phobos, as a function of its distance from Mars. At the current $d = 2.76\ R$, an angle of friction of 7.1° suffices. If it is a rubble pile with a friction angle of 30°, it will expand in an unbounded fashion at a distance of 2.12 times Mars's radius. Even very large friction angles would only allow existence to about 2.0 times Mars's radius.

is in the region where the smallest principal stress (most compressive) is along the y axis and the largest (least compressive) is along the x axis. For the angle of friction of 30°, $m = 3.0$ from Eq. (17). Therefore the velocity field upon yielding has the form

$$v_x = 3x\dot{\lambda}, \quad v_y = -y\dot{\lambda}, \quad v_z = 0, \tag{22}$$

so that it would expand along the largest x axis and contract along the intermediate y axis. There is no change along the shortest z axis. Thus it will become even more elongated when this yield occurs.

This change moves the state off of this plot. However, the detailed results of the analysis were used to determine the change in required friction angle for a small change in configuration of this type. Specifically, an increment value of $\Delta\lambda = 10^{-4}$ was assumed, which gives an increment in the largest semi-axis a of 3.99 m and a shortening of b by 1.1 m. That change of shape increases the rotary inertia and therefore decreases the spin accordingly. The original spin of $\omega = 3.3827 \times 10^{-4}$ rad/s decreases to $\omega = 3.38178 \times 10^{-4}$ rad/s. That new shape and spin have a required friction angle of 29.978°, so the deformation is initially stable. However, assuming that the rate at which the spin again achieves its resonance with its orbit is small compared to the time to move to closer ranges, then Phobos will spin up to its original value of $\omega = 3.3827 \times 10^{-4}$ rad/s. That state requires a friction angle of 30.01°; consequently Phobos will, in this ideal theory, fail during that phase of its evolution.

The expected fate of Phobos at that time would be a catastrophic and global disruption: it would fly apart in an expansion along its largest direction.

7. SUMMARY

Limits to equilibrium shapes for cohesionless solid bodies with self-gravitation and spin have been derived using a Mohr–Coloumb model. There is a range of shapes possible for each spin rate. The data for 845 known asteroids are compared to these limit curves. In almost all cases, the combination of spin rate and shape are well within equilibrium limits for fairly small values for the friction angle and well within the values typical of dry soils. Consequently, the shapes and spin states cannot be used to claim that the bodies must be cohesive; they are almost all consistent with a rubble-pile, moderate porosity structure. Phobos is used as an example showing how the theory also predicts the nature of any failure.

ACKNOWLEDGMENTS

The author acknowledges many useful discussions and substantial help from Kevin Housen. He is indebted to Alan Harris for furnishing the database on the asteroids. Thanks are due to Anthony Dobrovolskis and Erik Asphaugh for thorough reviews.

REFERENCES

Aggarwal, H. R., and V. R. Oberbeck 1974. Roche limit of a solid body. *Astrophys. J.* **191**, 577–588.

Chakrabarty, J. 1987. *Theory of Plasticity.* McGraw-Hill, New York.

Chandrasekhar, S. 1969. *Ellipsoidal Figures of Equilibrium*. Dover, New York.

Chen, W. F., and D. J. Han 1988. *Plasticity for Structural Engineers*. Springer-Verlag, Berlin/New York.

Chen, W. F., and H. Zhang 1991. *Structural Plasticity.* Springer-Verlag, Berlin/New York.

Chree, C. 1888. *Q. J. Math.* **23**.

Chree, C. 1891. *Phil. Mag. Ser. 5*, **32**.

Davidsson, B. J. R. 1999. Tidal splitting and rotational breakup of solid spheres. *Icarus* **142**, 525–535.

Dobrovolskis, A. R. 1982. Internal stresses in Phobos and other triaxial bodies. *Icarus* **52**, 136–148.

Harris, A. W. 1996. The rotation rates of very small asteroids: Evidence for "rubble-pile" structure. *Proc. Lunar Planet. Conf. 27th*, 493–494.

Jacobi, C. G. J. 1834. Über die figur des gleichgewichts. *Poggendorff Ann. Phys. Chem.* **33**, 229–238.

Jeffreys, H. 1947. The relation of cohesion to Roche's limit. *Mon. Nat. R. Astron. Soc.* **3**, 260–262.

Lambe, T. W., and R. V. Whitman 1969. *Soil Mechanics*. Wiley, New York.

Love, A. E. H. 1944. *A Treatise on the Mathematical Theory of Elasticity*. Dover, New York.

Maclaurin, C. 1742: see Todhunter, I. 1962. *History of the Mathematical Theories of Attraction and the Figure of the Earth*. Dover, New York.

Newton, I. 1687. Philosophiae Naturalis Principia Mathematica. (H. Pemberton, Ed.), 3rd edition. London.

Õpik, E. J. 1950. *Irish Astron. J.* **1**, 25–26.

Poincaré, H. 1885. Sur l'équilibre d'une masse fluide animée d'un mouvement de rotation. *Acta Math* **7**, 259–380.

Pravec, P., and A. W. Harris 2000. Fast and slow rotation of asteroids. *Icarus* **148**, 12–20.

Richardson, C., W. Bottke, and S. Love 1998. Tidal distortion and disruption of Earth-crossing asteroids. *Icarus* **134**, 47–76.

Roche, M. E. 1850. La figure d'une masse fluide. *Acad. Sci. Lettr. Montpellier* **1**, 243–262, 333–348.

Sekiguchi, N. 1970. On the fission of a solid body under influence of tidal force. *Moon* **1**, 429–439.

Slyuta, E. N., and S. A. Voropaev 1997. Gravitational deformation in shaping asteroids and small satellites. *Icarus* **129**, 401–414.